Temperature-Dependent $s_\pm \leftrightarrow s_{++}$ Transitions in the Multiband Model for Fe-Based Superconductors with Impurities

V. A. Shestakov [1], M. M. Korshunov [1,*] and O. V. Dolgov [2,3]

[1]   Kirensky Institute of Physics, Federal Research Center KSC SB RAS, 660036 Krasnoyarsk, Russia;
     v_shestakov@iph.krasn.ru
[2]   Donostia International Physics Center, 20018 Donostia-San Sebastian, Spain; oleg@dipc.org
[3]   P.N. Lebedev Physical Institute RAS, 119991 Moscow, Russia
[*]   Correspondence: mkor@iph.krasn.ru

Abstract: We study the dependence of the superconducting gaps on both the disorder and the temperature within the two-band model for iron-based materials. In the clean limit, the system is in the $s_\pm$ state with sign-changing gaps. Scattering by nonmagnetic impurities leads to the change of the sign of the smaller gap, resulting in a transition from the $s_\pm$ to the s_{++} state with the sign-preserving gaps. We show here that the transition is temperature-dependent. Thus, there is a line of $s_\pm \to s_{++}$ transition in the temperature–disorder phase diagram. There is a narrow range of impurity scattering rates, where the disorder-induced $s_\pm \to s_{++}$ transition occurs at low temperatures, but then the low-temperature s_{++} state transforms back to the $s_\pm$ state at higher temperatures. With increasing impurity scattering rate, the temperature of such $s_{++} \to s_\pm$ transition shifts to the critical temperature T_c, and only the s_{++} state is left for higher amounts of disorder.

Keywords: unconventional superconductors; iron pnictides; iron chalcogenides; impurity scattering

1. Introduction

Iron-based pnictides and chalcogenides attract a great deal of attention due to the presence of an unconventional superconducting state and peculiar normal state properties [1–8]. The electronic structure of these Fe-based high-T_c superconductors (FeBS) demonstrates several features that set them apart from other conventional and unconventional superconductors. First of all, most FeBS have similar Fermi surface topology that consists of two or three hole pockets centered at the $(0,0)$ point and two electron pockets centered at the (π, π) point of the Brillouin zone, corresponding to one Fe per unit cell. Exceptions are the cases of the extreme electron or hole doping, where only one group of sheets remains. A second important feature is that all five iron $3d$ orbitals contribute to the formation of the Fermi surface, and even a single Fermi pocket is formed by several d-orbitals. Thus, the system can only be described within a multiorbital and, respectively, a multiband model. A minimal model would be a two-band model, as suggested in Refs. [9–11]. The third interesting feature is connected with the unconventional superconductivity. While there is generally some controversy in the discussion of the gap symmetry in unconventional superconductors, growing evidence in iron-based materials supports the sign-changing gap. The structure of the Fermi surface provides practically ideal nesting at the antiferromagnetic wave vector $\mathbf{Q} = (\pi, \pi)$. The long-range spin-density wave antiferromagnetic state is destroyed by doping, but the enhanced spin fluctuations remain. These fluctuations are claimed to be the main source of the Cooper pairing, thus contributing to the formation of the superconducting ground state [5,8,12]. Since spin fluctuations with the large wave vector $\sim \mathbf{Q}$ lead to the repulsive interband Cooper interaction, the gap function must possess

momentum dependence and must change sign between the hole and the electron Fermi surface pockets to compensate the sign of the interaction in the gap equation. The simplest solution is called the $s_\pm$ state, and corresponds to the A_{1g} representation with the gap having one sign at hole pockets and opposite sign at electron pockets. At the same time, bands near the Fermi level have a mixed orbital character. Therefore, orbital fluctuations enhanced by, for example, electron–phonon interaction may also lead to a superconductivity [13–15]. These two mechanisms of superconducting pairing differ in the dominating superconducting gap structure: sign-changing $s_\pm$ state for the spin fluctuations and sign-preserving s_{++} state for the orbital fluctuations. Unfortunately, the superconducting gap structure has not yet been convincingly determined in experiments. Nevertheless, a series of experimental observations such as the spin resonance peak in inelastic neutron scattering [16–19], a quasiparticle interference in tunneling experiments [20–23], the NMR spin-lattice relaxation rate [24,25], and the temperature dependence of the penetration depth [26–28] are conveniently explained assuming the $s_\pm$ state.

Scattering on nonmagnetic impurities has different effects on superconductors with different gap symmetries and structures. The pure attractive interaction, both in the intraband and interband channels, results in the s_{++} state. Its reaction to the disorder has been well-known since the earlier studies of the conventional s-wave superconductivity [29,30] and the modern treatment of the s_{++} state within the multiband models [31]. According to the so-called Anderson's theorem [29], in a single-band s-wave superconductor, a nonmagnetic disorder does not affect the superconducting critical temperature T_c. In the case of unconventional superconductors, Anderson's theorem is violated and the critical temperature is suppressed by a nonmagnetic disorder [32], similar to the T_c suppression according to the Abrikosov–Gor'kov theory for magnetic impurities [33]. However, a series of experiments on FeBS revealed that this suppression is less intensive than predicted by the Abrikosov–Gor'kov theory [34–38]. One possible reason is that the $s_\pm$ state transforms to the s_{++} state at some critical value of the impurity scattering rate Γ^{crit} [10,11,39,40]. The latter is proportional to the impurity potential and the concentration of impurities n_{imp}. The transition occurs when one of the gaps (the smaller one) decreases and then changes its sign, going through zero. This generally happens due to the presence of the subdominant attractive intraband interactions in addition to the dominant interband repulsion, resulting in the $s_\pm$ state in the clean case [11].

In our previous studies [10,11,41,42], we have mostly discussed the low-temperature behavior of the superconducting gaps. Here we study the effect of nonmagnetic disorder on the two-band $s_\pm$ superconductor for a wide temperature range up to T_c. We show that there is a range of Γ's near Γ^{crit}, where although the smaller gap changed its sign at low temperatures (s_{++} state), at higher temperatures the sign was changed back and the system again became of $s_\pm$ type, staying in this state up to T_c.

2. Model and Method

Here we used the same two-band model as in Refs. [10,11,42] with the following Hamiltonian:

$$H = \sum_{\mathbf{k},\alpha,\sigma} \xi_{\mathbf{k},\alpha} c^\dagger_{\mathbf{k}\alpha\sigma} c_{\mathbf{k}\alpha\sigma} + \sum_{\mathbf{R}_i,\sigma,\alpha,\beta} \mathcal{U}^{\alpha\beta}_{\mathbf{R}_i} c^\dagger_{\mathbf{R}_i\alpha\sigma} c_{\mathbf{R}_i\beta\sigma} + H_{SC}, \tag{1}$$

where the operator $c^\dagger_{\mathbf{k}\alpha\sigma}$ ($c_{\mathbf{k}\alpha\sigma}$) creates (annihilates) an electron with momentum $\mathbf{k}$, spin σ, and band index $\alpha = a, b$, $\xi_{\mathbf{k},\alpha} = \mathbf{v}_{F\alpha}(\mathbf{k} - \mathbf{k}_{F\alpha})$ is the quasiparticles' dispersion linearized near the Fermi level with $\mathbf{v}_{F\alpha}$ and $\mathbf{k}_{F\alpha}$ being the Fermi velocity and the Fermi momentum of the band α, respectively. The Hamiltonian contains the term with the impurity potential $\mathcal{U}$ at site $\mathbf{R}_i$ and the term responsible for superconductivity, H_{SC}. The exact form of the latter is not important for the present discussion, but we assume that it provides superconducting pairing due to the exchange of spin fluctuations (repulsive interaction) and electron–phonon coupling (attractive interaction). See details in Ref. [11].

To describe the effect of disorder, we use the Eliashberg approach for multiband superconductors [43]. The connection between the full Green's function $\hat{\mathbf{G}}(\mathbf{k}, \omega_n)$, the self-energy matrix $\hat{\mathbf{\Sigma}}(\mathbf{k}, \omega_n)$, and the "bare" Green's function,

$$\hat{G}^{(0)\alpha\beta}(\mathbf{k}, \omega_n) = \left(i\omega_n\hat{\tau}_0 \otimes \hat{\sigma}_0 - \xi_{\mathbf{k}\alpha}\hat{\tau}_3 \otimes \hat{\sigma}_0\right)^{-1}\delta_{\alpha\beta}, \tag{2}$$

is established via the Dyson equation, $\hat{\mathbf{G}}(\mathbf{k}, \omega_n) = \left(\hat{\mathbf{G}}^{(0)-1}(\mathbf{k}, \omega_n) - \hat{\mathbf{\Sigma}}(\mathbf{k}, \omega_n)\right)^{-1}$, where $\omega_n = (2n+1)\pi T$ is Matsubara frequency. Green's function is the matrix in the band space (denoted by bold face) and combined Nambu and spin spaces (denoted by hat). The Pauli matrices $\hat{\tau}_i$ and $\hat{\sigma}_i$ refer to Nambu and spin spaces, respectively.

Assuming the isotropic superconducting gaps at the Fermi surface sheets, we set the impurity self-energy to be independent of the momentum $\mathbf{k}$ but preserving the dependence on the frequency and the band indices,

$$\hat{\mathbf{\Sigma}}(\omega_n) = \sum_{i=0}^{3} \Sigma_{(i)\alpha\beta}(\omega_n)\hat{\tau}_i. \tag{3}$$

Therefore, the task is simplified by averaging over $\mathbf{k}$. As a result, all equations are written in terms of the quasiclassical ξ-integrated Green's functions,

$$\hat{\mathbf{g}}(\omega_n) = \int d\xi(\mathbf{k})\hat{G}(\mathbf{k}, \omega_n) = \begin{pmatrix} \hat{g}_{an} & 0 \\ 0 & \hat{g}_{bn} \end{pmatrix}, \tag{4}$$

where

$$\hat{g}_{\alpha n} = g_{0\alpha n}\hat{\tau}_0 \otimes \hat{\sigma}_0 + g_{2\alpha n}\hat{\tau}_2 \otimes \hat{\sigma}_2. \tag{5}$$

Here $g_{0\alpha n}$ and $g_{2\alpha n}$ are the normal and anomalous (Gor'kov) ξ-integrated Green's functions in the Nambu representation,

$$g_{0\alpha n} = -\frac{i\pi N_\alpha \tilde{\omega}_{\alpha n}}{\sqrt{\tilde{\omega}_{\alpha n}^2 + \tilde{\phi}_{\alpha n}^2}}, \qquad\qquad g_{2\alpha n} = -\frac{\pi N_\alpha \tilde{\phi}_{\alpha n}}{\sqrt{\tilde{\omega}_{\alpha n}^2 + \tilde{\phi}_{\alpha n}^2}}. \tag{6}$$

They depend on the density of states per spin at the Fermi level of the corresponding band ($N_{a,b}$), and on the order parameter $\tilde{\phi}_{\alpha n}$ and frequency $\tilde{\omega}_{\alpha n}$. Both the order parameter and the frequency are renormalized by the self-energy,

$$i\tilde{\omega}_{\alpha n} = i\omega_n - \Sigma_{0\alpha}(\omega_n) - \Sigma_{0\alpha}^{\text{imp}}(\omega_n), \tag{7}$$

$$\tilde{\phi}_{\alpha n} = \Sigma_{2\alpha}(\omega_n) + \Sigma_{2\alpha}^{\text{imp}}(\omega_n), \tag{8}$$

where $\Sigma_{0(2)\alpha}$ and $\Sigma_{0(2)\alpha}^{\text{imp}}$ are the parts of the self-energy coming from the pairing interaction (spin fluctuations, electron–phonon coupling, etc.) and impurity scattering, respectively. Impurity scattering will be considered in the *s*-wave channel only. Treating a more complicated impurity potential is a separate cumbersome task, although this goal was pursued by some authors [44–46]. The order parameter $\tilde{\phi}_{\alpha n}$ is connected with the gap function $\Delta_{\alpha n}$ via the renormalization factor $Z_{\alpha n} = \tilde{\omega}_{\alpha n}/\omega_n$. That is,

$$\Delta_{\alpha n} = \tilde{\phi}_{\alpha n}/Z_{\alpha n}. \tag{9}$$

The part of the self-energy due to the pairing interaction can be written as

$$\Sigma_{0\alpha}(\omega_n) = T \sum_{n',\beta} \lambda^Z_{\alpha\beta}(n-n') \frac{g_{0\beta n'}}{N_\beta}, \tag{10}$$

$$\Sigma_{2\alpha}(\omega_n) = -T \sum_{n',\beta} \lambda^\phi_{\alpha\beta}(n-n') \frac{g_{2\beta n'}}{N_\beta}, \tag{11}$$

where $\lambda^{\phi,Z}_{\alpha\beta}(n-n')$ is a coupling function,

$$\lambda^{\phi,Z}_{\alpha\beta}(n-n') = 2\lambda^{\phi,Z}_{\alpha\beta} \int_0^\infty d\Omega \frac{\Omega B(\Omega)}{(\omega_n - \omega_{n'})^2 + \Omega^2}, \tag{12}$$

which is defined by coupling constants $\lambda^{\phi,Z}_{\alpha\beta}$ and includes density of states N_β and the normalized bosonic spectral function $B(\Omega)$. The matrix elements $\lambda^\phi_{\alpha\beta}$ may be positive (attractive) or negative (repulsive) due to Coulomb repulsion, spin fluctuations, and electron–phonon interaction, while matrix elements $\lambda^Z_{\alpha\beta}$ are always positive. For simplicity, we set $\lambda^Z_{\alpha\beta} = \left|\lambda^\phi_{\alpha\beta}\right| \equiv |\lambda_{\alpha\beta}|$.

To calculate the impurity part of the self-energy $\hat{\Sigma}^{\mathrm{imp}}$, we use noncrossing diagrammatic approximation that is equivalent to the $\mathcal{T}$-matrix approximation,

$$\hat{\Sigma}^{\mathrm{imp}}(\omega_n) = n_{\mathrm{imp}}\hat{U} + \hat{U}\hat{g}(\omega_n)\hat{\Sigma}^{\mathrm{imp}}(\omega_n), \tag{13}$$

where $\hat{U} = \mathbf{U} \otimes \hat{\tau}_3$ is the matrix of the impurity potential, $(\mathbf{U})_{\alpha\beta} = \mathcal{U}^{\alpha\beta}_{\mathbf{R}_i}$. Without loss of generality, we set $\mathbf{R}_i = 0$. Intra- and interband parts of the impurity potential are given as v and u, respectively, $(\mathbf{U})_{\alpha\beta} = (v-u)\delta_{\alpha\beta} + u$. The relation between intra- and interband impurity scattering is set by a parameter $\eta = v/u$.

It is convenient to introduce the generalized cross-section parameter

$$\sigma = \frac{\pi^2 N_a N_b u^2}{1 + \pi^2 N_a N_b u^2} \rightarrow \begin{cases} 0, & \text{Born limit,} \\ 1, & \text{unitary limit} \end{cases} \tag{14}$$

and the impurity scattering rate

$$\Gamma_{a(b)} = 2n_{\mathrm{imp}} \pi N_{b(a)} u^2 (1-\sigma) = \frac{2n_{\mathrm{imp}}\sigma}{\pi N_{a(b)}} \rightarrow \begin{cases} 2n_{\mathrm{imp}} \pi N_{b(a)} u^2, \text{Born limit,} \\ \dfrac{2n_{\mathrm{imp}}}{\pi N_{a(b)}}, \text{unitary limit.} \end{cases} \tag{15}$$

Both are shown to have special values in the limiting cases: (i) the Born limit corresponding to the weak impurity potential ($\pi u N_{a(b)} \ll 1$), and (ii) the unitary limit corresponding to the strong impurity potential ($\pi u N_{a(b)} \gg 1$).

The equations presented above are general and can be applied to a wide range of multiband systems. Below we concentrate on iron-based superconductors within the minimal two-band model. Bands are labelled as a and b. The spin fluctuation spectrum enters through the bosonic spectral function $B(\Omega)$ [47–49]; the superconducting interaction is also determined by the choice of the coupling constants $\lambda_{\alpha\beta}$.

3. Results and Discussion

For the calculations, we chose the ratio between densities of states of different bands as $N_b/N_a = 2$ and set the values of the coupling constants to be $(\lambda_{aa}; \lambda_{ab}; \lambda_{ba}; \lambda_{bb}) = (3; -0.2; -0.1; 0.5)$, so the averaged coupling constant is positive, $\langle\lambda\rangle = (\lambda_{aa} + \lambda_{ab})N_a/N + (\lambda_{ba} + \lambda_{bb})N_b/N > 0$, where $N = N_a + N_b$. This set of parameters leads to the $s_\pm$ superconducting state with unequal gaps—larger positive (band a) and smaller negative (band b) gap—and the critical temperature $T_{c0} = 40$ K in the clean limit.

We present the smaller gap $\Delta_{b,n}$ for the lowest Matsubara frequency, $n = 0$, as a function of the scattering rate Γ_a and the temperature T in two different cases: (i) weak scattering with $\sigma = 0$ (Born limit), see Figure 1; and (ii) intermediate scattering limit with $\sigma = 0.5$, see Figure 2. The larger gap, $\Delta_{a,n}$, is always positive, and therefore, there is a line of $s_{\pm} \rightarrow s_{++}$ transition corresponding to the change of the $\Delta_{b,n}$ sign from negative to positive. The transition goes through the gapless state with the finite larger gap and the vanishing smaller gap [10]. Note that the line of transition is not vertical in Figures 1 and 2. Therefore, there is no single critical scattering rate, but a temperature-dependent $\Gamma_a^{\text{crit}}(T)$. Moreover, if we stay at a fixed Γ_a in the range $1.1T_{c0} < \Gamma_a < 1.6T_{c0}$ for $\sigma = 0$ or $1.5T_{c0} < \Gamma_a < 3.2T_{c0}$ for $\sigma = 0.5$ and increase the temperature, we observe an interesting behavior of the gap. Namely, while at low temperatures the transition to the s_{++} state already took place ($\Delta_{b,n} > 0$). At higher temperatures, the system goes back to the $s_{\pm}$ state ($\Delta_{b,n} < 0$). Thus, there is a temperature-dependent $s_{++} \rightarrow s_{\pm}$ transition. With the increasing Γ_a, the temperature of this transition is shifted to T_c and the system becomes s_{++} for the whole temperature range.
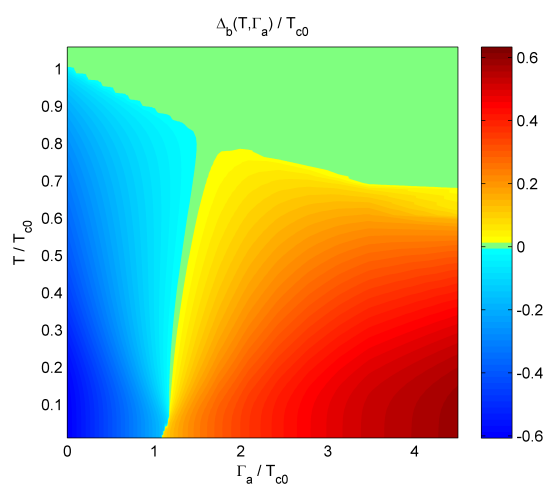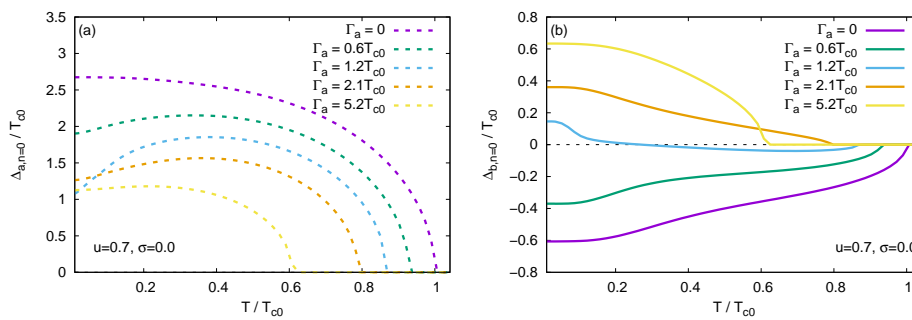

Figure 1. Dependence of the lowest-frequency Matsubara gap function $\Delta_{b,n=0}$, indicated by the color code, for the band b on the scattering rate Γ_a and the temperature T in the Born limit, $\sigma = 0.0$. All quantities are normalized by T_{c0}. Green color marks the state with the vanishingly small gap, $\Delta_{b,n} < 10^{-3}T_{c0}$.
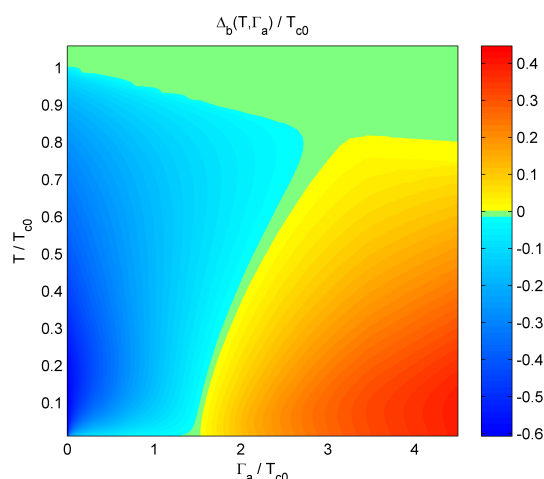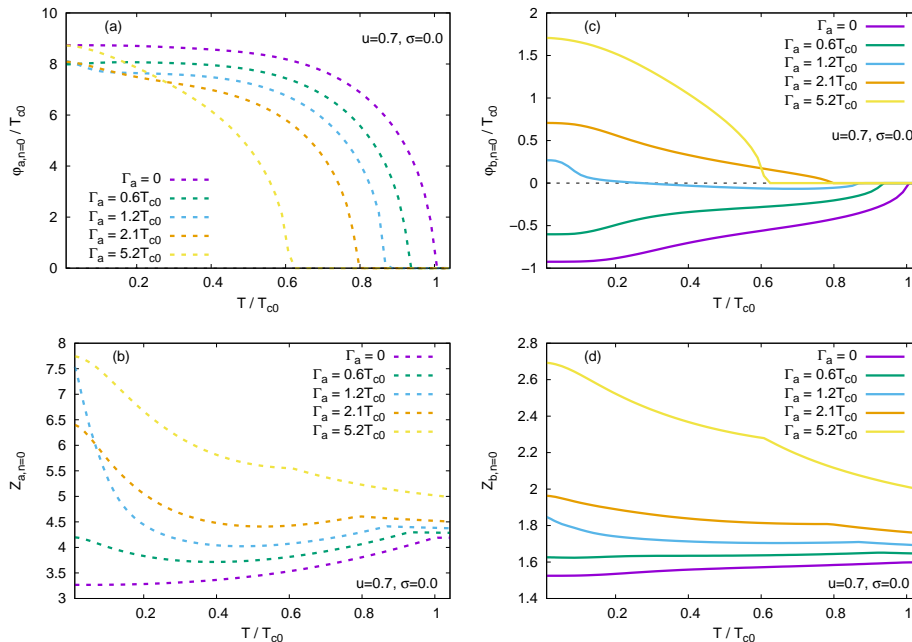

Figure 2. Dependence of the lowest-frequency Matsubara gap function $\Delta_{b,n=0}$, indicated by the color code, for the band b on Γ_a and T in the intermediate scattering limit, $\sigma = 0.5$. All quantities are normalized by T_{c0}. Green color marks the state with the vanishingly small gap, $\Delta_{b,n} < 10^{-3}T_{c0}$.

To illustrate the mentioned points, in Figures 3 and 4 we present results for the temperature dependence of the gap function $\Delta_{\alpha,n=0}$, order parameter $\tilde{\phi}_{\alpha,n=0}$, and the renormalization factor $Z_{\alpha,n=0}$

for several fixed values of Γ_a for $\sigma = 0$. Temperature dependencies for $\sigma = 0.5$ are shown in Figures 5 and 6. The gap in band a has the same positive sign for all values of Γ_a and vanishes at T_c (see Figures 3a and 5a). However, there is a small range of Γ_a values around Γ_a^{crit} for which the gap is an increasing function of T at low temperatures. At the same time, the order parameter behaves quite conventionally and decreases towards T_c (see Figures 4a and 6a). The unusual temperature dependence of the gap at the lowest Matsubara frequency is due to the renormalization factor $Z_{\alpha,n=0}$ that is shown in Figures 4b and 6b. That is, according to Equation (9), large values of $Z_{\alpha,n}$ taking place at low temperatures lead to the decrease of $\Delta_{\alpha,n}$. For the band b, the same effect is not seen in the Born limit, but becomes pronounced in the intermediate scattering limit. Compare the gap function in Figure 5b and the order parameter in Figure 6c, and also notice the low-temperature behavior of $Z_{\alpha,n}$ in Figure 6d. In principle, similar gap behavior may occur from the functional form of gaps at real frequencies (see Equation (7) in Ref. [50]).
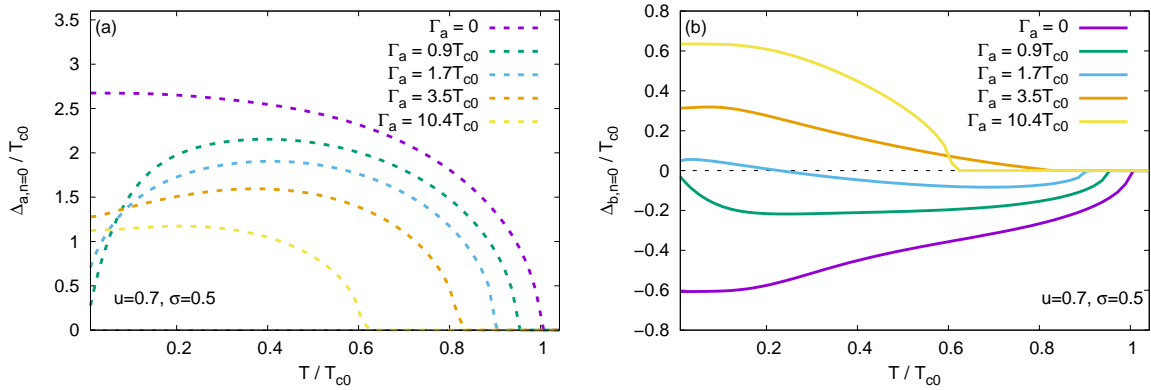

Figure 3. Temperature dependence of the lowest-frequency Matsubara gap $\Delta_{\alpha,n=0}$ normalized by T_{c0} for fixed values of Γ_a in the Born limit with the band index (**a**) $\alpha = a$ and (**b**) $\alpha = b$.
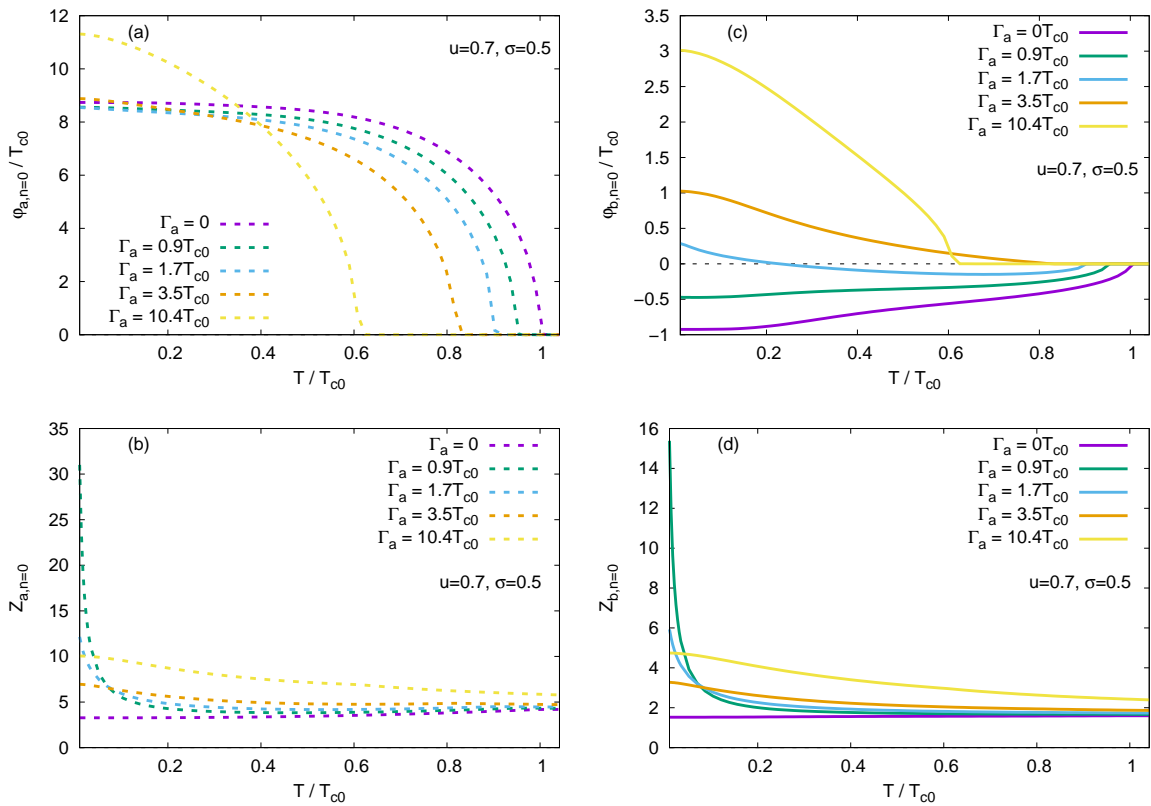

Figure 4. Temperature dependence of the lowest-frequency Matsubara order parameter $\tilde{\phi}_{\alpha,n=0}$ (**a**,**c**) and the renormalization factor $Z_{\alpha,n=0}$ (**b**,**d**), both normalized by T_{c0}, for fixed values of Γ_a in the Born limit with the band index $\alpha = a$ (**a**,**b**) and $\alpha = b$ (**c**,**d**).

In the clean limit and for small Γ_a, the sign of the smaller gap $\Delta_{b,n}$ is negative at all temperatures (see Figures 3b and 5b). With the increase of the impurity scattering rate, the gap at low temperatures

changes sign while at higher temperatures the sign is either reversed again (small Γ_a) or the gap vanishes ($\Gamma_a \gtrsim 2T_{c0}$). Therefore, the transition from the $s_\pm$ state to the s_{++} state is characterized by two parameters: the critical scattering rate Γ_a^{crit} and the critical temperature T^{crit}. The latter changes from zero to T_c. Thus, the s_{++} state becomes dominant in the initially clean $s_\pm$ system for $\Gamma_a > \Gamma_a^{\mathrm{crit}}$ and $T < T^{\mathrm{crit}}$. This is true in both Born limit and the intermediate scattering limit. We also checked that the similar behavior holds for the higher Matsubara frequencies (see Figure 7 for the illustration of the gaps behavior for $n = 1$ and $n = 10$).
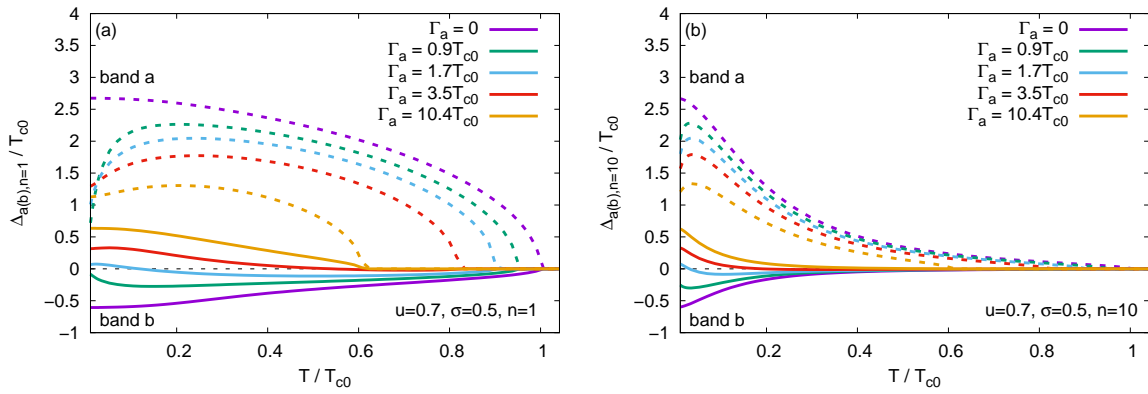

Figure 5. Temperature dependence of the lowest-frequency Matsubara gap $\Delta_{\alpha,n=0}$ normalized by T_{c0} for fixed values of Γ_a in the intermediate scattering limit ($\sigma = 0.5$) with the band index (**a**) $\alpha = a$ and (**b**) $\alpha = b$.
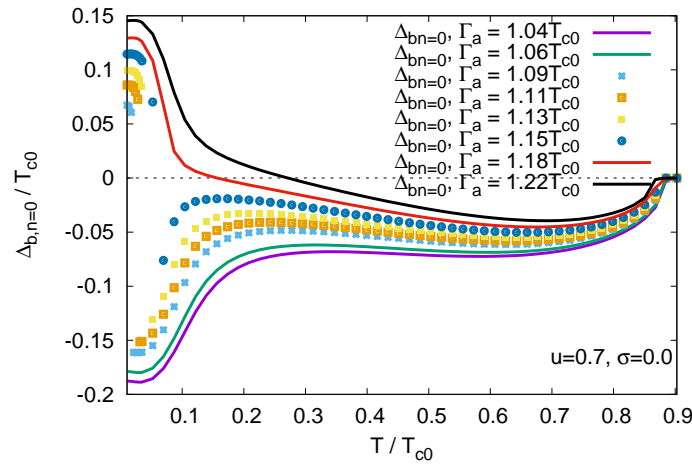

Figure 6. Temperature dependence of the lowest-frequency Matsubara order parameter $\tilde{\phi}_{\alpha,n=0}$ (**a,c**) and the renormalization factor $Z_{\alpha,n=0}$ (**b,d**), both normalized by T_{c0}, for fixed values of Γ_a in the intermediate scattering limit ($\sigma = 0.5$) with the band index $\alpha = a$ (a,b) and $\alpha = b$ (c,d).

Figure 7. Temperature dependence of the gap for higher Matsubara frequencies, (**a**) $\Delta_{\alpha,n=1}$ and (**b**) $\Delta_{\alpha,n=10}$, normalized by T_{c0} for fixed values of Γ_a in the intermediate scattering limit ($\sigma = 0.5$). Gaps corresponding to the band index a (band index b) are shown by dashed (solid) curves.

Previously, we found a steep change in the smaller gap as a function of the scattering rate in the weak scattering limit [42]. Here we observe that the same jump is present in the temperature dependence of the gap. See Figure 8, where $\Delta_{b,n}$ in the Born limit is shown. A discontinuous jump in the temperature dependence of the smaller gap appears at $T < 0.1T_{c0}$.

Figure 8. Temperature dependencies of lowest-frequency Matsubara gap $\Delta_{b,n=0}$ normalized by T_{c0} in the Born limit for several values of Γ_a. Solid curves correspond to a smooth evolution of the gap in the $s_{\pm}$ state and across the $s_{++} \rightarrow s_{\pm}$ transition, while the temperature dependencies with the discontinuous jump of the gap are shown by symbols.

4. Conclusions

We considered a two-band model for FeBS that has the $s_{\pm}$ superconducting ground state in the clean limit. Here we studied the dependence of the superconducting gaps $\Delta_{\alpha,n}$ on both the temperature and the nonmagnetic impurity scattering rate. We showed that the disorder-induced transition from $s_{\pm}$ to s_{++} state is temperature-dependent. That is, in a narrow region of scattering rates, while the ground state is s_{++}, it transforms back to the $s_{\pm}$ state at higher temperatures up to T_c. With the increasing impurity scattering rate, the temperature of such a $s_{++} \rightarrow s_{\pm}$ transition shifts to the critical temperature T_c. The $s_{\pm} \rightarrow s_{++}$ transition is characterized by two parameters: (i) the critical scattering rate Γ_a^{crit} and (ii) the critical temperature $T^{\text{crit}} \leq T_c$. The s_{++} state becomes dominant in the initially clean $s_{\pm}$ system for $\Gamma_a > \Gamma_a^{\text{crit}}$ and $T < T^{\text{crit}}$. A similar situation takes place for the case of the magnetic

disorder, where the $s_\pm$ state at low temperatures occurs due to the $s_{++} \to s_\pm$ transition [41], and at higher temperatures may transform back to the s_{++} state.

Experimentally, one can observe the re-entrant $s_\pm$ state by increasing the temperature for the fixed amount of disorder that results in the low-temperature s_{++} state. For example, the spin resonance peak in the inelastic neutron scattering should be absent in the low-temperature s_{++} state, but must appear in the $s_\pm$ state at higher temperatures [8,12,16,17]. The temperature dependence of the penetration depth should also bear specific signatures of the gapless behavior accompanying the $s_{++} \to s_\pm$ transition [11].

Author Contributions: All author contributed equally.

Conflicts of Interest: The authors declare no conflict of interest.

Abbreviations

The following abbreviations are used in this manuscript:

FeBS　　Fe-based superconductors
NMR　　nuclear magnetic resonance

References

1. Sadovskii, M.V. High-temperature superconductivity in iron-based layered iron compounds. *Phys. Usp.* **2008**, *51*, 1201. [CrossRef]
2. Izyumov, Y.A.; Kurmaev, E.Z. FeAs systems: A new class of high-temperature superconductors. *Phys. Usp.* **2008**, *51*, 1261–1286. [CrossRef]
3. Ivanovskii, A.L. New high-temperature superconductors based on rare-earth and transition metal oxyarsenides and related phases: synthesis, properties, and simulations. *Phys. Usp.* **2008**, *51*, 1229–1260. [CrossRef]
4. Paglione, J.; Greene, R.L. High-temperature superconductivity in iron-based materials. *Nat. Phys.* **2010**, *6*, 645–658. [CrossRef]
5. Mazin, I.I. Superconductivity gets an iron boost. *Nature* **2010**, *464*, 183–186. [CrossRef] [PubMed]
6. Wen, H.H.; Li, S. Materials and Novel Superconductivity in Iron Pnictide Superconductors. *Annu. Rev. Condens. Matter Phys.* **2011**, *2*, 121–140. [CrossRef]
7. Stewart, G.R. Superconductivity in iron compounds. *Rev. Mod. Phys.* **2011**, *83*, 1589–1652. [CrossRef]
8. Hirschfeld, P.J.; Korshunov, M.M.; Mazin, I.I. Gap symmetry and structure of Fe-based superconductors. *Rep. Prog. Phys.* **2011**, *74*, 124508. [CrossRef]
9. Raghu, S.; Qi, X.L.; Liu, C.X.; Scalapino, D.J.; Zhang, S.C. Minimal two-band model of the superconducting iron oxypnictides. *Phys. Rev. B* **2008**, *77*, 220503. [CrossRef]
10. Efremov, D.V.; Korshunov, M.M.; Dolgov, O.V.; Golubov, A.A.; Hirschfeld, P.J. Disorder-induced transition between $s_\pm$ and s_{++} states in two-band superconductors. *Phys. Rev. B* **2011**, *84*, 180512. [CrossRef]
11. Korshunov, M.M.; Togushova, Y.N.; Dolgov, O.V. Impurities in multiband superconductors. *Phys. Usp.* **2016**, *59*, 1211–1240. [CrossRef]
12. Korshunov, M.M. Superconducting state in iron-based materials and spin-fluctuation pairing theory. *Phys. Usp.* **2014**, *57*, 813. [CrossRef]
13. Kontani, H.; Onari, S. Orbital-Fluctuation-Mediated Superconductivity in Iron Pnictides: Analysis of the Five-Orbital Hubbard-Holstein Model. *Phys. Rev. Lett.* **2010**, *104*, 157001. [CrossRef] [PubMed]
14. Onari, S.; Kontani, H. Self-consistent Vertex Correction Analysis for Iron-based Superconductors: Mechanism of Coulomb Interaction-Driven Orbital Fluctuations. *Phys. Rev. Lett.* **2012**, *109*, 137001. [CrossRef] [PubMed]
15. Yamakawa, Y.; Kontani, H. Superconductivity without a hole pocket in electron-doped FeSe: Analysis beyond the Migdal-Eliashberg formalism. *Phys. Rev. B* **2017**, *96*, 045130. [CrossRef]

16. Maier, T.A.; Scalapino, D.J. Theory of neutron scattering as a probe of the superconducting gap in the iron pnictides. *Phys. Rev. B* **2008**, *78*, 020514. [CrossRef]

17. Korshunov, M.M.; Eremin, I. Theory of magnetic excitations in iron-based layered superconductors. *Phys. Rev. B* **2008**, *78*, 140509. [CrossRef]

18. Christianson, A.D.; Goremychkin, E.A.; Osborn, R.; Rosenkranz, S.; Lumsden, M.D.; Malliakas, C.D.; Todorov, I.S.; Claus, H.; Chung, D.Y.; Kanatzidis, M.G.; et al. Unconventional superconductivity in $Ba_{0.6}K_{0.4}Fe_2As_2$ from inelastic neutron scattering. *Nature* **2008**, *456*, 930–932. [CrossRef] [PubMed]

19. Inosov, D.S.; Park, J.T.; Bourges, P.; Sun, D.L.; Sidis, Y.; Schneidewind, A.; Hradil, K.; Haug, D.; Lin, C.T.; Keimer, B.; et al. Normal-state spin dynamics and temperature-dependent spin-resonance energy in optimally doped $BaFe_{1.85}Co_{0.15}As_2$. *Nat. Phys.* **2010**, *6*, 178–181. [CrossRef]

20. Wang, Y.L.; Shan, L.; Fang, L.; Cheng, P.; Ren, C.; Wen, H.H. Multiple gaps in $SmFeAsO_{0.9}F_{0.1}$ revealed by point-contact spectroscopy. *Supercond. Sci. Technol.* **2009**, *22*, 015018. [CrossRef]

21. Gonnelli, R.; Daghero, D.; Tortello, M.; Ummarino, G.; Stepanov, V.; Kremer, R.; Kim, J.; Zhigadlo, N.; Karpinski, J. Point-contact Andreev-reflection spectroscopy in ReFeAsO1-xFx (Re = La, Sm): Possible evidence for two nodeless gaps. *Phys. C Supercond.* **2009**, *469*, 512–520. [CrossRef]

22. Szabó, P.; Pribulová, Z.; Pristáš, G.; Bud'ko, S.L.; Canfield, P.C.; Samuely, P. Evidence for two-gap superconductivity in $Ba_{0.55}K_{0.45}Fe_2As_2$ from directional point-contact Andreev-reflection spectroscopy. *Phys. Rev. B* **2009**, *79*, 012503. [CrossRef]

23. Zhang, X.; Lee, B.; Khim, S.; Kim, K.H.; Greene, R.L.; Takeuchi, I. Probing the order parameter of superconducting LiFeAs using Pb/LiFeAs and Au/LiFeAs point-contact spectroscopy. *Phys. Rev. B* **2012**, *85*, 094521. [CrossRef]

24. Nakai, Y.; Kitagawa, S.; Ishida, K.; Kamihara, Y.; Hirano, M.; Hosono, H. Systematic ^{75}As NMR study of the dependence of low-lying excitations on F doping in the iron oxypnictide $LaFeAsO_{1-x}F_x$. *Phys. Rev. B* **2009**, *79*, 212506. [CrossRef]

25. Fukazawa, H.; Yamazaki, T.; Kondo, K.; Kohori, Y.; Takeshita, N.; Shirage, P.M.; Kihou, K.; Miyazawa, K.; Kito, H.; Eisaki, H.; et al. 75As NMR Study of Hole-Doped Superconductor Ba1-xFxFe2As2 (Tc≃38 K). *J. Phys. Soc. Jpn.* **2009**, *78*, 033704. [CrossRef]

26. Ghigo, G.; Ummarino, G.A.; Gozzelino, L.; Gerbaldo, R.; Laviano, F.; Torsello, D.; Tamegai, T. Effects of disorder induced by heavy-ion irradiation on $(Ba_{1-x}K_x)Fe_2As_2$ single crystals, within the three-band Eliashberg $s\pm$ wave model. *Sci. Rep.* **2017**, *7*, 13029. [CrossRef] [PubMed]

27. Ghigo, G.; Ummarino, G.A.; Gozzelino, L.; Tamegai, T. Penetration depth of $\mathbf{Ba_{1-x}K_xFe_2As_2}$ single crystals explained within a multiband Eliashberg $s\pm$ approach. *Phys. Rev. B* **2017**, *96*, 014501. [CrossRef]

28. Teknowijoyo, S.; Cho, K.; Kończykowski, M.; Timmons, E.I.; Tanatar, M.A.; Meier, W.R.; Xu, M.; Bud'ko, S.L.; Canfield, P.C.; Prozorov, R. Robust $s_\pm$ pairing in $CaK(Fe_{1-x}Ni_x)_4As_4$ ($x = 0$ and 0.05) from the response to electron irradiation. *Phys. Rev. B* **2018**, *97*, 140508. [CrossRef]

29. Anderson, P. Theory of dirty superconductors. *J. Phys. Chem. Solids* **1959**, *11*, 26–30. [CrossRef]

30. Morosov, A.I. Static impurities in a highly anisotropic superconductor. *Fiz. Tverd. Tela* **1979**, *21*, 3598–3600.

31. Onari, S.; Kontani, H. Violation of Anderson's Theorem for the Sign-Reversing *s*-Wave State of Iron-Pnictide Superconductors. *Phys. Rev. Lett.* **2009**, *103*, 177001. [CrossRef] [PubMed]

32. Golubov, A.A.; Mazin, I.I. Effect of magnetic and nonmagnetic impurities on highly anisotropic superconductivity. *Phys. Rev. B* **1997**, *55*, 15146–15152. [CrossRef]

33. Abrikosov, A.A.; Gor'kov, L.P. Contribution to the theory of superconducting alloys with paramagnetic impurities. *Sov. Phys. JETP* **1961**, *12*, 1243–1253.

34. Karkin, A.E.; Werner, J.; Behr, G.; Goshchitskii, B.N. Neutron-irradiation effects in polycrystalline $LaFeAsO_{0.9}F_{0.1}$ superconductors. *Phys. Rev. B* **2009**, *80*, 174512. [CrossRef]

35. Cheng, P.; Shen, B.; Hu, J.; Wen, H.H. Contrasting impurity scattering and pair-breaking effects by doping Mn and Zn in $Ba_{0.5}K_{0.5}Fe_2As_2$. *Phys. Rev. B* **2010**, *81*, 174529. [CrossRef]

36. Li, Y.; Tong, J.; Tao, Q.; Feng, C.; Cao, G.; Chen, W.; Zhang, F.-c.; Xu, Z-a. Effect of a Zn impurity on T c and its implications for pairing symmetry in $LaFeAsO_{1-x}F_x$. *New J. Phys.* **2010**, *12*, 083008. [CrossRef]

37. Nakajima, Y.; Taen, T.; Tsuchiya, Y.; Tamegai, T.; Kitamura, H.; Murakami, T. Suppression of the critical temperature of superconducting $Ba(Fe_{1-x}Co_x)_2As_2$ by point defects from proton irradiation. *Phys. Rev. B* **2010**, *82*, 220504. [CrossRef]

38.　Prozorov, R.; Kończykowski, M.; Tanatar, M.A.; Thaler, A.; Bud'ko, S.L.; Canfield, P.C.; Mishra, V.; Hirschfeld, P.J. Effect of Electron Irradiation on Superconductivity in Single Crystals of Ba$(Fe_{1-x}Ru_x)_2As_2$ ($x = 0.24$). *Phys. Rev. X* **2014**, *4*, 041032. [CrossRef]

39.　Yao, Z.J.; Chen, W.Q.; Li, Y.k.; Cao, G.h.; Jiang, H.M.; Wang, Q.E.; Xu, Z.a.; Zhang, F.C. Zn-impurity effect and interplay of $s_\pm$ and s_{++} pairings in iron-based superconductors. *Phys. Rev. B* **2012**, *86*, 184515. [CrossRef]

40.　Chen, H.; Tai, Y.Y.; Ting, C.S.; Graf, M.J.; Dai, J.; Zhu, J.X. Disorder effects in multiorbital $s_\pm$-wave superconductors: Implications for Zn-doped $BaFe_2As_2$ compounds. *Phys. Rev. B* **2013**, *88*, 184509. [CrossRef]

41.　Korshunov, M.M.; Efremov, D.V.; Golubov, A.A.; Dolgov, O.V. Unexpected impact of magnetic disorder on multiband superconductivity. *Phys. Rev. B* **2014**, *90*, 134517. [CrossRef]

42.　Shestakov, V.A.; Korshunov, M.M.; Togushova, Y.N.; Efremov, D.V.; Dolgov, O.V. Details of the disorder-induced transition between s $\pm$ and s ++ states in the two-band model for Fe-based superconductors. *Supercond. Sci. Technol.* **2018**, *31*, 034001. [CrossRef]

43.　Allen, P.B.; Mitrovic, B. Theory of Superconducting T_c. *Solid State Phys. Adv. Res. Appl.* **1982**, *37*, 1–92. [CrossRef]

44.　Hoyer, M.; Scheurer, M.S.; Syzranov, S.V.; Schmalian, J. Pair breaking due to orbital magnetism in iron-based superconductors. *Phys. Rev. B* **2015**, *91*, 054501. [CrossRef]

45.　Scheurer, M.S.; Hoyer, M.; Schmalian, J. Pair breaking in multiorbital superconductors: An application to oxide interfaces. *Phys. Rev. B* **2015**, *92*, 014518. [CrossRef]

46.　Pogorelov, Y.G.; Loktev, V.M. Conventional and unconvenstional impurity effects in superconductors (Review Article). *Low Temp. Phys.* **2018**, *44*, 1–28. [CrossRef]

47.　Parker, D.; Dolgov, O.V.; Korshunov, M.M.; Golubov, A.A.; Mazin, I.I. Extended $s_\pm$ scenario for the nuclear spin-lattice relaxation rate in superconducting pnictides. *Phys. Rev. B* **2008**, *78*, 134524. [CrossRef]

48.　Popovich, P.; Boris, A.V.; Dolgov, O.V.; Golubov, A.A.; Sun, D.L.; Lin, C.T.; Kremer, R.K.; Keimer, B. Specific Heat Measurements of $Ba_{0.68}K_{0.32}Fe_2As_2$ Single Crystals: Evidence for a Multiband Strong-Coupling Superconducting State. *Phys. Rev. Lett.* **2010**, *105*, 027003. [CrossRef] [PubMed]

49.　Charnukha, A.; Dolgov, O.V.; Golubov, A.A.; Matiks, Y.; Sun, D.L.; Lin, C.T.; Keimer, B.; Boris, A.V. Eliashberg approach to infrared anomalies induced by the superconducting state of $Ba_{0.68}K_{0.32}Fe_2As_2$ single crystals. *Phys. Rev. B* **2011**, *84*, 174511. [CrossRef]

50.　Mikhailovsky, A.A.; Shulga, S.V.; Karakozov, A.E.; Dolgov, O.V.; Maksimov, E.G. Thermal pair-breaking in superconductors with strong electron-phonon interaction. *Solid State Commun.* **1991**, *80*, 511–515. [CrossRef]